Use of a genetic algorithm to improve predictions of alternate bar dynamics

M. A. F. Knaapen and S. J. M. H. Hulscher

Water Engineering and Management, Department of Engineering Technology, University of Twente, Enschede, Netherlands

Received 24 October 2002; revised 24 April 2003; accepted 21 May 2003; published 4 September 2003.

[1] Alternate bars may form in sandy beds of straight rivers and channels. These bars are characterized by the alternation of crests, all moving downstream at a speed of several meters per day. The aim of this paper is to predict the dynamics of alternate bars. To that end, we tested predictions of measured alternate bars in flume experiments, as derived from an amplitude evolution model. Weakly nonlinear stability analysis underlies this amplitude evolution model, so that it applies to situations in which the width-to-depth ratio is close to the critical ratio, above which alternate bars occur. The experiments have a width-to-depth ratio far above the critical value, well outside the range of formal validity of the model. While wavelengths and heights of the alternate bars are still well predicted, we found that the migration rate is not: the amplitude evolution model produces an underestimation of close to a factor of two. Therefore we took a slightly different approach. We tested the predictive capability for this amplitude evolution model by using a genetic algorithm to tune the model to bathymetric data. After tuning, the model is indeed able to predict the migration rate of the bars over periods that exceed the tuning period by far. Limits to the prediction time, i.e., failure of this method, could not be derived for the data sets used in this work. *INDEX TERMS:* 1815 Hydrology: Erosion and sedimentation; 1824 Hydrology: Geomorphology (1625); 3210 Mathematical Geophysics: Modeling; *KEYWORDS:* morphology, alternate bars, data assimilation, genetic algorithm, optimization, modeling

Citation: Knaapen, M. A. F., and S. J. M. H. Hulscher, Use of a genetic algorithm to improve predictions of alternate bar dynamics, *Water Resour. Res.*, *39*(9), 1231, doi:10.1029/2002WR001793, 2003.

1. Introduction

[2] The interaction between a noncohesive bed and water motion results in interesting phenomena. Several types of wavy patterns can develop on sandy beds. Alternate bars are the largest free bed forms observed in fixed-bank rivers and channels. This bar pattern consists of an alternation of crests and troughs between the channel banks (see Figure 1). The wavelength of the bars is several times the width of the river, while the height is up to several meters. Alternate bars have been observed in rivers worldwide: for example the Tokachi in Japan (Figure 1), the Jamuna [*Ashworth et al.*, 2000] in Bangladesh, the Rhine in Switzerland, and in North Boulder Creek, [*Furbish et al.*, 1998] in the USA.

[3] The existence of alternate bars is thought to reflect an inherent instability of the bed and depth-averaged-flow system. This system has a straight forward equilibrium state, a spatially uniform river bed with a constant longitudinal slope and a constant flow over it. However, under certain conditions this state is unstable. Under these conditions, the interaction of the flow with the sand results in rhythmic bed patterns like ripples, dunes, or alternate bars.

[4] Such instabilities can be modeled using a stability analysis. The equilibrium state is disturbed by infinitesimal perturbations with a wide range of wavelengths. In the linear stability analysis, the growth rates of these perturbations are examined based on the linearization of the flow and sediment transport equations. For most conditions, all perturbations have negative growth rates and the bed will stay flat. For certain conditions, some perturbations have positive growth rates. If the model is correct, the wavelength of these waves should correspond to the observed bed pattern, alternate bars in our case.

[5] As the linear approximation is invalid once the amplitude of the perturbations are no longer infinitesimally, this approach is unable to describe the actual dynamics of the waves. This purpose requires a weakly nonlinear analysis. Next to the linear terms in the equations, the 2nd and 3rd order approximation of the system equations are evaluated. Consequently, the system is valid for larger perturbations as well. Both *Colombini et al.* [1987] and *Schielen et al.* [1993] assessed such a nonlinear stability analysis for alternate bars in rivers, resulting in an amplitude evolution model describing the slow temporal variations of the bar in time. The latter model is an extension of the former as it also accounts for large-scale spatial variations in the amplitude.

[6] The advantage of a stability approach over a straight forward numerical analysis is twofold. Firstly, the stability analysis is based on simplified equations, that are solved analytically. The equations contain the bare elements necessary to represent the solution. Consequently, this approach gives good insight on the relevant physical processes, whereas numerical model results are more difficult to analyze. Second, the analytical approach is inherently

Copyright 2003 by the American Geophysical Union.
0043-1397/03/2002WR001793$09.00

Figure 1. Tokachi River, Japan. The flow is from top to bottom. Photo Hokkaido Development Bureau, courtesy of K. Sato.

stable, while in every numerical model it is difficult to find the right balance between allowing for perturbation growth and noise reduction. So far, no numerical model has been published that is able to describe the long term evolution of free rhythmic bed features.

[7] The amplitude evolution models, resulting from the stability analysis, describe the dynamics of alternate bars in rivers. So far, however, there has been no evidence that the amplitude evolution models can also predict these dynamics of alternate bars. The predictability, in a deterministic sense, of the small-scale morphodynamic processes is restricted in time [*De Vriend*, 1998, 2001]. Because of the recursive interactions, even smallest errors in the sediment transport models eventually become unacceptably large. However, the large-scale changes in themselves may still have fairly regular, and to some extent predictable, properties. We think that the amplitude evolution models resulting from a stability analysis can be used to predict these large-scale changes. In this paper we test this idea for alternate bar dynamics using the flume experiments of *Lanzoni* [2000b, 2000a].

[8] To utilize the amplitude evolution model for predictions of alternate bar dynamics, accurate estimates of both the initial state and the model parameters are required. Theoretical values of the parameters have been found to result in good estimates of both the wavelength and the height of alternate bars [*Knaapen et al.*, 2001]. However, those studies did not consider bar dynamics. As this paper will show, the model tuned with theoretical parameters does not predict accurate migration rates.

[9] Therefore a data assimilation procedure, called genetic algorithm, is used to find those parameter values that do result in accurate migration rates. Data assimilation is the science in which available measurements are used to optimize predictive models. This approach is now often used in oceanography [*Canizares et al.*, 1998; *Voorrips et al.*, 1999; *Van Leeuwen*, 1999; *Feddersen and Guza*, 2000; *Heemink et al.*, 2002; *Leredde et al.*, 2002; *Moore et al.*, 2002; *Knaapen and Hulscher*, 2002; *Morelissen et al.*, 2003].

[10] The genetic algorithm finds those parameter values that give the best fit to part of the available data. Starting from a random initial set of model parameter combinations, the genetic algorithm combines and modifies the parameters. This algorithm, that resembles genetic reproduction in biology, results in a model that predicts the remaining measurements accurately.

[11] This paper is organized as follows. First the genetic algorithm is explained in section 2. Section 3 describes the flume experiments that are used to test the amplitude evolution model. The model predictions based on theoretical parameters are evaluated in section 5, while in section 6, the model is tuned using the genetic algorithm. Section 8 describes possible applications of the amplitude evolution model combined with a genetic algorithm. Our findings are summarized in section 9.

2. Using a Genetic Algorithm for Data Assimilation

[12] Data assimilation is the mathematical science to incorporate measurements into models.

[13] With online data assimilation, the model with an initial set of parameters is used to make predictions. During the predictions, the model variables and parameters are changed every time new data show discrepancies between the model and the data. This changes of the parameters depend on the difference between the predicted and the measured values. The main advantage of online data assimilation is that it allows parameters to vary in time. The main disadvantage is that online techniques only work if the model and the initial parameters already are fairly accurate. In our problem the initial accuracy of the model is limited as will be shown in section 5. For a thorough introduction, the interested reader is referred to *Anderson* [1979] or *Lewis* [1986]. *Canizares et al.* [1998], *Voorrips et al.* [1999], and *Van Leeuwen* [1999] all give applications of online data assimilation in physical oceanographic problems.

[14] Off-line data assimilation, in general referred to as optimization algorithms [see *Fletcher*, 1987], aim to find the best values for both the parameters and the initial state of a model relative to measured data. In general, these algorithms are based on a gradient analysis. The dependency of the model results to the parameters is analyzed using the derivatives of the model. On the basis of the derivatives the best parameter change is chosen. A state-of-the-art example of the gradient search is the adjoint approach (see *Heemink et al.* [2002], *Leredde et al.* [2002], and *Moore et al.* [2002] for applications in oceanography).

[15] Because of the nonlinearity of our model and the amount of noise on the measurement data, the problem has many local minima. Consequently, gradient search algorithms are not always effective, because they are very sensitive to the occurrence of such local minima. Therefore we use a global optimization routine. Global optimizers aim to find the minimum of any function, regardless of its properties. Although efforts are made to construct deterministic global optimizers, most global optimizers are based on a stochastic search. A genetic algorithm is one type of global optimizer.

[16] In a genetic algorithm, all unknown parameters are gathered in a vector. A vector with allowed parameter values is referred to as ''individual'', while a collection of vectors is named ''population''. For each individual, a model run is executed using the parameter values of the individual. Each individual receives a fitness parameter, which is the root-mean-square difference between the measured bathymetry and the bathymetry predicted by the model using the parameter values of that individual (RSME).

[17] At the start of the algorithm, a population of individuals is generated with random parameter values, with uniform parameter distributions within imposed boundaries. From this initial population, new individuals are produced, analogously to genetic reproduction. A new individual can be created through two types of operations. With crossover, parameter values from two individuals are exchanged. Mutation is the operation in which one or more parameter values of a single individual are changed. Because of the reproduction, the population grows.

[18] However, some individuals die, thereby reducing the population size. Each individual has a chance on survival, depending on its fitness. The fittest individuals, with a low RMSE, have a better chance on survival than individuals with high RMSEs. Thus new populations are generated iteratively. According to this approach, the genetic algorithm explores the whole parameter domain. The combination of the genetic reproduction and the survival of the fittest is able to identify the areas with low RMSEs. These promising areas are explored more extensively than other areas. The only thing left to do is to identify which individual has the lowest RMSE. This individual contains an optimal parameter combination.

[19] In principle, this approach is not effected by local minima. However, since the approach partly depends on chance, one might end up in a local minimum, especially in the case of a model with numerous local minima. Therefore it is preferred to repeat the algorithm a number of times. The best result will then be the global minimum. Alternatively, one could start a final run with the local minima as initial guess.

[20] *Davis* [1991] gives a more complete discussion of genetic algorithms, and *Knaapen and Hulscher* [2002] use a genetic algorithm in a marine morphology problem.

3. Large-Scale Flume Experiments on Alternate Bars

[21] In 1995, *Lanzoni* [2000b, 2000a] generated alternate bars under steady flow conditions in the large, straight sand flume of WL|Delft Hydraulics. The flume was 1.5 m wide, 1 m deep and 50 m long. The bathymetry was measured over a length of 43.8 m.

[22] During the experiments, all flow characteristics were controlled. Both the water level and the water flux were kept constant at the values chosen for the experiments. Sand leaving the flume was weighed and subsequently fed back at the upstream end of the flume, evenly distributed over the flume's width.

[23] From the series of experiments [*Lanzoni*, 2000b, 2000a], two were selected to test the amplitude evolution model. Experiment P1801 is a very long test (816 h) with relatively deep water (7.3 cm) and low flow velocities (0.27 m/s). This run was part of the series with uniform size sediment (d_{50} = 481 μm, d_{90} = 710 μm, ρ_s = 2650 kg/m^3).

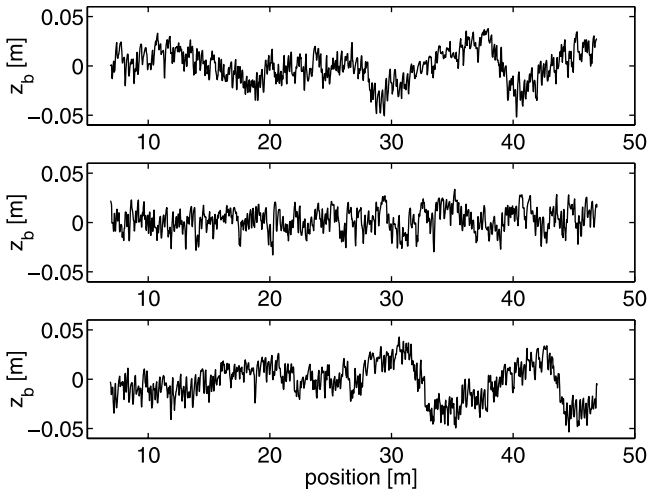

Figure 2. Longitudinal bed profile measured during experiment P1801. From top to bottom: the profiles along a section near the left bank, at the central line, and near the right bank of the flume.

[24] Experiment P0109 is much shorter (51 hours), and had shallower water (4.7 cm) and higher flow velocities (0.57 m/s). This run was part of the series with graded sediment (d_{50} = 262 μm, d_{90} = 3210 μm, ρ_s = 2650 kg/m^3).

[25] A water level indicator and a profile indicator measured the water level and the bed profile respectively. In brief periods of 4 to 6 min, measurements were taken along three longitudinal sections, one along the central line and the other two at 0.20 m from each wall. At the end of an experiment, bed profiles were taken at 0.40 and 0.60 m from each wall. The interval between consecutive measurements depends on the rate of the morphological change.

[26] Figure 2 shows an example of the three resulting longitudinal bed profiles. Each crest on one side of the flume clearly corresponds with a trough on the opposing side. Ripples, which can be up to 2 cm high, appear as noise in the bathymetry.

[27] The measurements of the water level and the bed level can be used to determine the water depth: $h_\star = \zeta - \tilde{z}_b$, in which $\tilde{z}_b$ and ζ are the bed level and the water level, respectively. For each section, the average longitudinal bed slope (i_{b1}, i_{b2}, i_{b3}) is calculated using linear regression.

[28] The Chézy coefficient can be estimated from the measured water depth, by using:

$$C_z = \frac{u}{\sqrt{h_\star i_b}} \tag{1}$$

in which $h_\star$ is the water depth, averaged over time and space, $i_b = (i_{b1}, i_{b2}, i_{b3})/3$ the mean bed slope, and u the flow velocity averaged over time and space.

4. Amplitude Evolution Model

[29] Stability analysis approaches have been used for a variety of morphodynamic problems in rivers [*Ikeda et al.*, 1981; *Colombini et al.*, 1987; *Johannesson and Parker*,

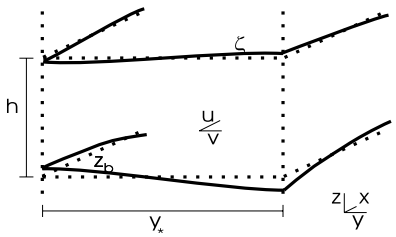

Figure 3. Sketch explaining the definitions that are used in the derivation of the predictive model.

1989; *Schielen et al.*, 1993; *Furbish*, 1998; *Seminara et al.*, 2001]. Also see *Dodd et al.* [2003] for an overview of stability analysis applied to the marine environment.

[30] We use the morphodynamic equations of *Schielen et al.* [1993] to describe the dynamics of alternate bars in rivers. These equations describe a uniform, shallow-water flow in an infinitely long straight channel with a uniformly mild slope (see the definition sketch in Figure 3). We assume the banks to be nonerodible and the bottom sediment to be noncohesive. The flow is described using the mass balance and the depth-averaged St. Venant equations, in which the friction at the bed is modeled using a drag coefficient. The sediment is assumed to be transported as bed load, which is modeled with a generic formula:

$$S = \sigma |U|^b \left(\frac{U}{|U|} - \gamma \nabla z_b \right) \tag{2}$$

In which S is the amount of sediment transported, U is the flow velocity vector and z_b is the deviation from the mean bed level. Parameter σ denotes the proportionality of transport, b determines the nonlinearity of the transport as a function of the depth, while γ denotes the bed slope effect.

[31] A weakly nonlinear stability analysis of this equation resulted in the following amplitude evolution model describing the deviation of the bed as a traveling wave:

$$z_b(x, y, t) = h_\star \epsilon A(\xi, \tau) e^{ikx + \omega t} \cos(\pi y) + NLT + c.c. \tag{3}$$

in which (x, y) determine the position and t denotes time. Furthermore, ϵ is a small dimensionless parameter, while k and ω are the wave number and frequency, respectively. The cosine in equation (3) models the cross-stream variation of the crest, *c.c.* denotes the complex conjugates and *NLT* indicates the nonlinear terms (see Appendix A for the exact formulations).

[32] The amplitude $A(\xi, \tau)$ follows from:

$$\frac{\partial A}{\partial \tau} = \alpha_0 A + \alpha_1 \frac{\partial^2 A}{\partial \xi^2} + \alpha_2 |A|^2 A \tag{4}$$

which is known as the Ginzburg-Landau equation. The coefficients α_i (i = 0, 1, 2) in equation (4) are complex functions of the drag coefficient C_d and the transport parameters b and γ (see Appendix A for the exact formulations of *Schielen et al.* [1993]). Furthermore, τ is the morphological time and ξ is the spatial morphological coordinate in a frame moving with the group speed ν_k of the bars:

$$\tau = \epsilon^2 t, \qquad \xi = \epsilon(x + \nu_k t) \tag{5}$$

The group speed follows from the weakly nonlinear model as explained in Appendix A.

5. Predictions With Theoretical Parameters

[33] To use this amplitude evolution model for predicting bed level changes with time, we need values for the coefficients α_i (i = 0, 1, 2) of equation (4), all parameters in equation (3) as well as an initial state. According to *Schielen et al.* [1993], however, all coefficients and parameters are functions of the known width-to-depth ratio R, the drag-coefficient C_d and the transport parameters b, γ and σ.

[34] According to *Knaapen et al.* [2001], the parameters C_d, b, γ are accurately represented by:

$$C_d = \frac{g}{C_z^2} = \frac{g i_b h_\star}{u_\star^2} \tag{6}$$

$$b \approx \frac{3}{1 - \dfrac{\theta_c}{\mu\theta}} \tag{7}$$

$$\gamma \approx 0.75 \left(\frac{\theta_c}{\mu\theta} \right)^{\frac{1}{4}} \tag{8}$$

where C_z is the Chézy coefficient and θ and θ_c are the Shields parameter and the critical Shields parameter, respectively. Furthermore, μ is the bed form or efficiency factor.

[35] In their analysis, *Knaapen et al.* [2001] used the results of *Sekine and Parker* [1992] to find the value for γ. Equation (7) is derived from the *Meyer-Peter and Müller* [1948] formula for bed load transport. The proportionality parameter σ can also be estimated using this formula. After some calculations and using equation (6) one finds:

$$\sigma \approx 13.3 \sqrt{g \Delta d_{50}^3 (\mu\theta - \theta_c)^3 \left(\frac{C_d}{g \Delta \theta d_{50}} \right)} \tag{9}$$

in which Δ is the relative submerged weight of the sediment and d_{50} the median grain size.

[36] The migration rate c_b can be calculated from the model frequency ω and wave number k using:

$$c_b = -\frac{\omega}{k} = \frac{i\omega_c - \omega_{nl}}{k_c + k_{nl}} = \frac{i\omega_c - \epsilon \nu_k K - \epsilon^2 W}{k_c + \epsilon K} \tag{10}$$

In this equation, ω_c and wave number k_c are the critical values of ω and k, respectively. The critical values are the

Table 1. Parameters and Coefficients for the Conditions of the Experiments of *Lanzoni* [2000b, 2000a]

	α_0	α_1	α_2	ω_c	$min(\omega_{nl})$	$max(\omega_{nl})$	k_c	$min(k_{nl})$	$max(k_{nl})$
P1801	1.44 – 0.44i	0.35 – 1.04i	−5.21 – 1.73i	−1.10i	0.62	1.51	0.92	−0.17	0.17
P0109	0.48 – 0.13i	0.11 – 0.38i	−2.19 – 0.23i	−0.91i	−1.55	1.17	0.85	−0.85	0.91

wavelength and frequency of the fastest growing mode resulting from the linear stability analysis, which can be computed directly (see Appendix A). According tho the weakly nonlinear theory, the actual wavelength and frequency are close to these critical values. The real-valued nonlinear terms (W, K), are caused by the amplitude variations G described by the Ginzburg-Landau equation and are determined by:

$$Re(\alpha_0) + Re(\alpha_1)K^2 + Re(\alpha_2)G^2 = 0 \tag{11}$$

$$Im(\alpha_0) + Im(\alpha_1)K^2 + Im(\alpha_2)G^2 = W \tag{12}$$

This system is under-determined (2 equations, 3 variables: K, G, W). However, the range of possible wave number variations can be estimated using:

$$K^2 < Re(\alpha_0)f_e \tag{13}$$

with f_e a known function of α_i, $i = 1, 2$ [see *Schielen et al.*, 1993, equation (5.11)]. With this range estimate we can calculate the ranges of the nonlinear terms (W, K). Table 1 gives the values of the parameters α_i, $i = 0,1,2$ and the frequency components for the conditions of two experiments by *Lanzoni*, [2000b, 2000a].

[37] *Knaapen et al.* [2001], the computed migration rates are compared with the migration rates measured in the experiments of *Lanzoni* [2000b, 2000a]. Figure 4 clearly shows that the observed migration is well outside the range of possible migration rates predicted by the amplitude evolution model. The estimated sediment discharges $Q = S_x y_\star \left(\text{in}\left[\frac{m^3}{h}\right]\right)$, however, are in good agreement with the measured discharges (Figure 5).

[38] The difference between the predicted migration rates and measured values can be explained from the assumption of weak nonlinearity, on which the amplitude evolution model of *Schielen et al.* [1993] is based. On the basis of this assumption, they derived the complex frequency by using an expansion around the critical values (k_c, R_c). However, the real width-to-depth ratios R in the experiments are far above the critical values R_c (see Figure 6). Therefore the linear estimates are invalid, and we need a different approach for estimating the frequency and thus indirectly the migration rates.

6. Predictions With the Model and a Genetic Algorithm

[39] In practice, we are often interested in (low order) general information on alternate bars. For navigation purposes, for example, it is sufficient to know where the bars are located. From section 5 we know that the model is unable to predict such information using theoretical parameters, it under-estimates the migration rates considerably. Therefore in this section a genetic algorithm tunes a simplified version of the amplitude model to predict the average shape and the migration of bars in Lanzoni's experiments.

[40] In addition we will neglect all temporal variations of the amplitude. On the basis of the observed pattern in the experiments (Figure 2), we assume that the spatial variation in the amplitude of the alternate bars is a boundary effect. This boundary effect is included,

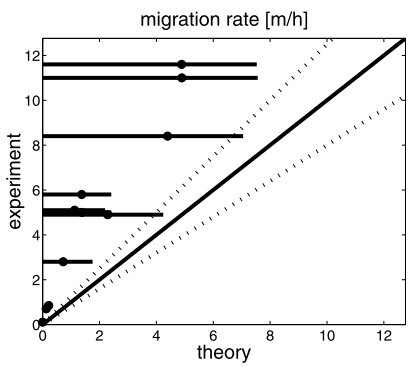

Figure 4. Prediction versus measurements: migration c_b (the dots give the value for $K = 0$, and the horizontal bars give the range of possible values).

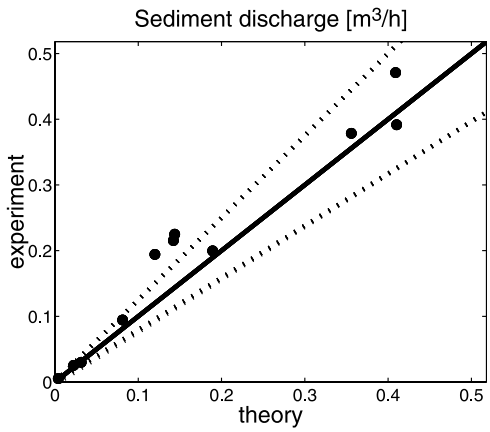

Figure 5. Prediction versus measurements: sediment discharge Q (the dashed lines show the 25% error boundaries).

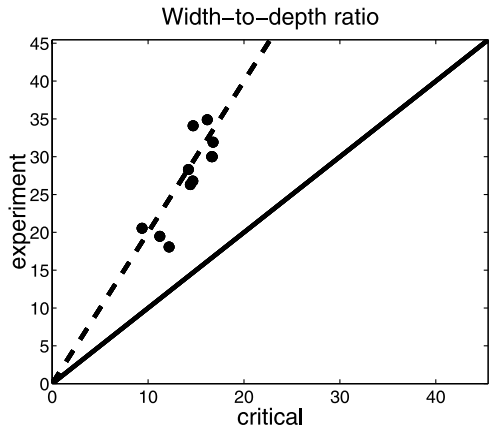

Figure 6. Prediction versus measurements: the real width-to-depth ratio against the critical width-to-depth ratio. All true ratios are about twice the critical value (dashed line).

through an exponential growth curve η in the bed form equation (3):

$$z_b = \epsilon h_\star \eta(x)\cos(k_c x + i\omega t + \phi_0)\cos(\pi y) + NLT + c.c.$$

$$\eta = 1 - exp\left(\frac{-c_2}{1-\left(\frac{x}{\max(x)}\right)^{c_1}}\right) \tag{14}$$

[41] In this data assimilation model, a simplified version of the amplitude evolution model, the average depth $h_\star$, position x and time t are known. Frequency ω, phase ϕ_0 and boundary effect parameters, c_1, c_2, should be estimated using the genetic algorithm. The higher order terms *NLT* are similar to the terms in the original model (see Appendix A), whereas ε and wave number k_c can be calculated directly from theory. *Knaapen et al.* [2001] show that this gives accurate estimates for the wavelength and amplitude. To increase the accuracy, the genetic algorithm is allowed to correct all parameters within a 25% margin of their theoretical values.

[42] Note that we use the wave frequency ω instead of the migration rate $c_b = \frac{-\omega}{k}$. Also note that the initial value problem is reduced to one unknown ϕ_0. The boundary relaxation is probably not optimal, but it does allow for both initial exponential growth and exponential decay. Since we are not interested in relaxation effects, this choice suffices.

[43] Lanzoni was interested in the initial development of alternate bars and his experiments were stopped when the amplitudes of the bars reached an equilibrium height. However, the data assimilation model assumes a constant amplitude. This restriction reduces the available data. We used the data assimilation model in equation (14) to predict the dynamics of alternate bars in experiments P1801 with uniform sand [*Lanzoni*, 2000b] and P0109 with graded sand [*Lanzoni*, 2000a].

[44] Of Lanzoni's experiment P1801, starting on 16 February 1995, at 16:08 hours, a number of measurements are used to tune the model. It turns out that even with only two surveys, taken just 9 min after each other, accurate

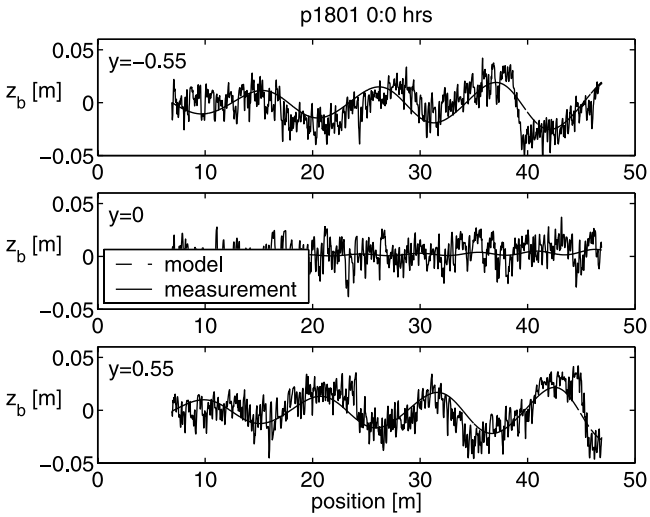

Figure 7. The last hindcast result compared to the measured bathymetry at the end of the tuning period ($t = 0$) in test P1801. The header gives the date and time of the measurement.

predictions can be made. After the tuning, the model predicted the bed topography for over 100 hours. We compare the predicted bathymetry to the measurements and conclude that the model predicts the measured bathymetry well (Figures 7, 8, and 9). At all times, the model predicts the peaks and the troughs at the correct locations and reproduces the shape bars accurate as well. Almost everywhere, the prediction errors are smaller than the ripples that are observed in the measurements.

[45] Furthermore, the differences between the predicted bathymetry and the measured values do not seem to change with time, which implies that the prediction error does not increase in time. This observation is confirmed by Figure 10. The dimensionless error (scaled by the measured amplitude) increases only marginally and, across the entire time domain, is about 20% larger than the standard deviation of

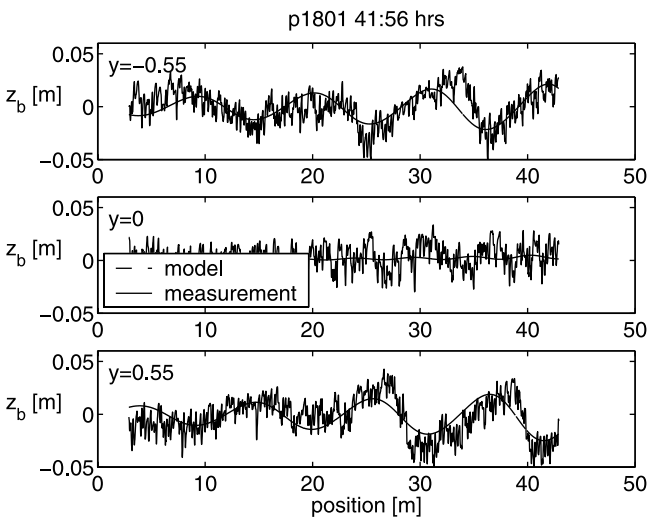

Figure 8. The model results compared to the measured bathymetry in test P1801. The header gives the date and time of the measurement.

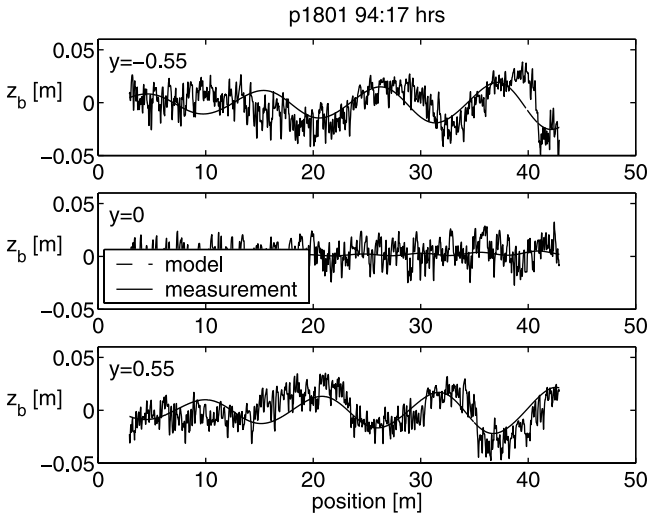

Figure 9. The model results compared to the measured bathymetry in test P1801. The header gives the date and time of the measurement.

the measurement noise. Small-scale bed perturbations, like ripples or dunes, cause most of the noise.

[46] Of Lanzoni's experiment P0109, two measurements are used to tune the data assimilation model. For this experiment the minimal required tuning period is 15 min, starting on September 1, 1995, at 11:00. After tuning, the model predicted the bed changes for the following 1:45 hours. Figures 11, 12, and 13 show the results. The only available shorter tuning period, 7.5 min results in an significant 20% increase of the error after 1 hour of predictions (Figure 14). This additional error is caused by an under-prediction of the propagation speed of the bars, which becomes significant within one period already.

[47] The alternate bars are less regular than those of experiment p1801. The model predicts the positions of the bars and the troughs correctly, but there appear to be some

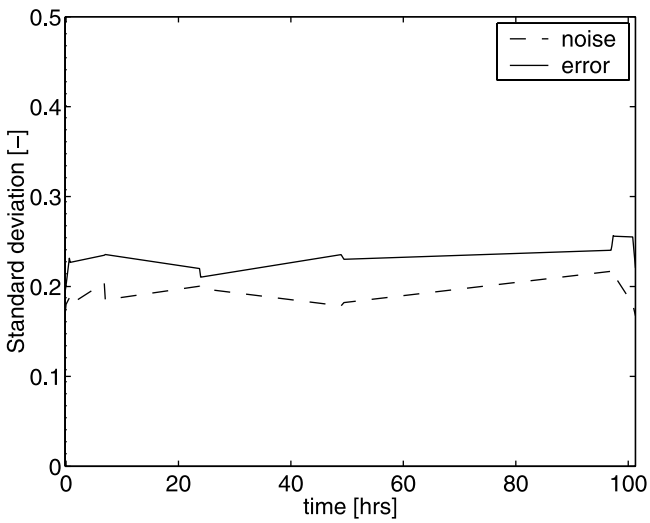

Figure 10. The root mean square error (E_{rms}, solid line) compared to an estimate of the standard deviation of the measurement noise (dashed line) for test P1801. Both quantities are scaled by the measured amplitude of the alternate bars.

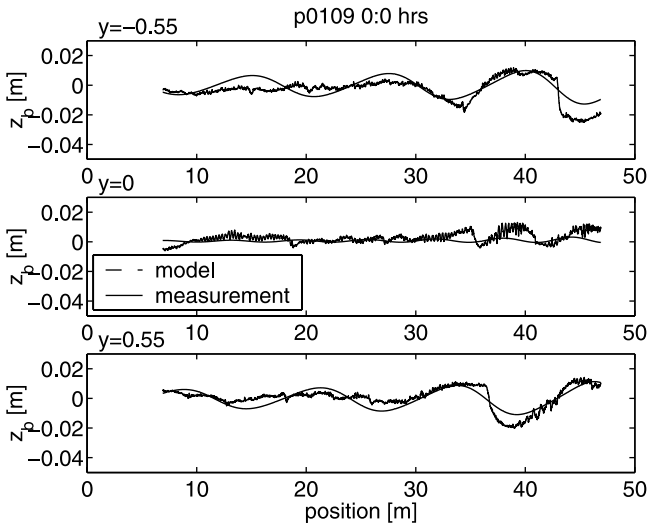

Figure 11. The last hindcast results compared to the measured bathymetry at the last hindcast resulting from the tuning (t = 0) in test P0109.

amplitude modulations. However, there is not enough spatial variation to link these variations to the amplitude evolution model. Still, the differences between the predicted and the measured bathymetry are small in the downstream part of the flume. The statistics of the results of P0109 (Figure 14) are similar to those of test P1801. The errors are about 50% larger than the measurement noise, but now the difference between the errors and the noise slowly increases with time.

7. Discussion of the Results

[48] For both tests, the differences between the predicted and the measured bathymetry are mainly related to the longitudinal asymmetry of the alternate bars. It is unlikely that higher order terms make up for this difference. It is probably another effect of the weakly nonlinear approach. Under the assumptions of near criticality, the nonlinearity of

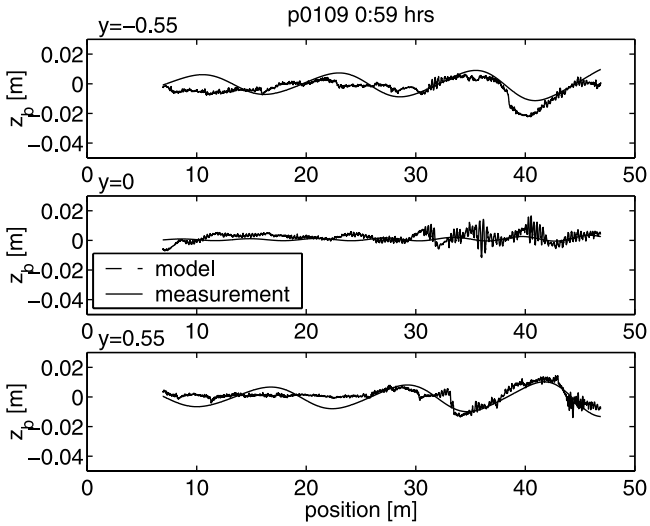

Figure 12. The model prediction compared to the measured bathymetry in test P0109 at the time indicated.

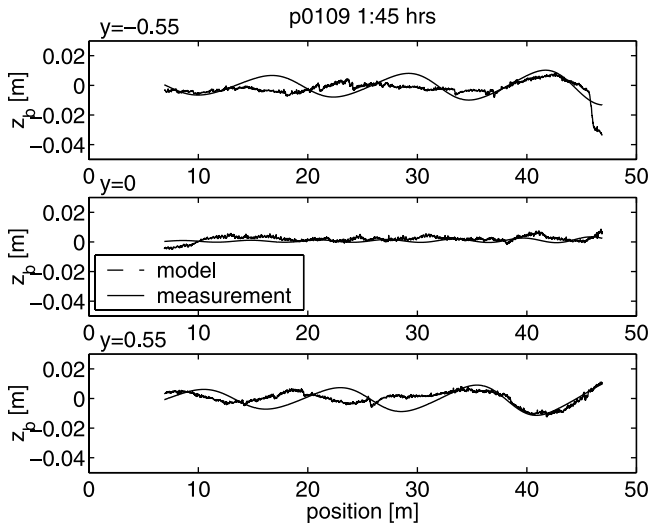

Figure 13. The model prediction compared to the measured bathymetry in test P0109 at the time indicated.

the system is insufficiently included in the model to describe the very steep fronts of the bars. In addition, a large part of the errors results from the boundary effect on the wavelength of the bars. This boundary effect was not imbedded in the amplitude relaxation in equation (14), but is clearly present in the graded-sediment experiment (P0109).

[49] For experiment P1801, the data assimilation model predicts a migration rate of about 2.9 m/day. This is slightly higher than reported by [*Lanzoni*, 2000b]: 2.6 m/day. For experiment P0109, the model optimizer led to a migration rate of about 8.8 m/hour, which again is a bit higher than the value of 8.4 m/hour, found by [*Lanzoni*, 2000b]. These differences appear to be well within the error margins of the model. Note that the estimates of the Lanzoni experiments were based on the displacement of the crests only. Our estimate is based on the complete profiles of the bars.

[50] The data assimilation model gives accurate predictions for the uniform-sand experiment P1801. The prediction error is slightly larger than the measurement noise for at least 1 wave period, after the model was tuned during only a marginally period (only 0.15% of the wave period). In experiment P0109 with graded sediment, the tuning time was 18% of the wave period. The predictions turn out to be still acceptable after 1.25 wave periods. In this experiment, reducing the tuning period to 9% of the wave period gave unreliable results. Probably the relatively large amplitude modulations increase the required tuning time.

[51] However, it can be concluded that only a short tuning time is required to get a long prediction window. In both tests, the standard deviation of the error increases only marginally with time. This suggests that the predictions stay accurate for a while. The actual prediction window will be much larger than the values found here. Unfortunately, it is impossible to test the accuracy of the predictions over a longer period, as no additional measurements are available.

8. Applicability of Data Assimilation Models in Morphodynamics

[52] In general, straight river channels are convenient for the purpose of navigation. However, when alternate bars occur in the channel, the river authorities have to indicate the navigation channel by using marks. Since the bars migrate downstream at a speed of several meters per day, the channel markings have to be updated frequently. Without a model, every update has to be based on time-consuming bathymetric surveys. With the data assimilation model presented in this paper, the number of measurements can be reduced, without increasing the risk to navigation.

[53] The combination of amplitude evolution models and data assimilation is promising. Stability analyses are performed on a wide range of rhythmic morphodynamic phenomena [*Dodd et al.*, 2003]. In some cases it is necessary to predict the dynamics of these changes. *Knaapen and Hulscher* [2002] for example, model the regeneration of dredged sand waves in a navigation channel. Data assimilation is an ideal tool for combining amplitude evolution models with available (remote sensing) data. The combination results in a fast and simple predictive model, even if full knowledge about the dynamical processes is incomplete.

9. Conclusions

[54] The derivation of *Schielen et al.* [1993] assumes a width-to-depth ratio that is near its critical value. However, in the experiments of *Lanzoni* [2000b] the width-to-depth ratio is at least twice its critical value. Consequently, the approximation is formally invalid for the conditions of the experiments. Nevertheless, *Knaapen et al.* [2001] show that the model is able to estimate the wavelength and height. The current paper shows that this approach leads to largely underestimated migration rates. Apparently, The size of the alternate bars is not affected under strongly nonlinear conditions, whereas the dynamics of the bars do change significantly when the conditions are no longer weakly nonlinear.

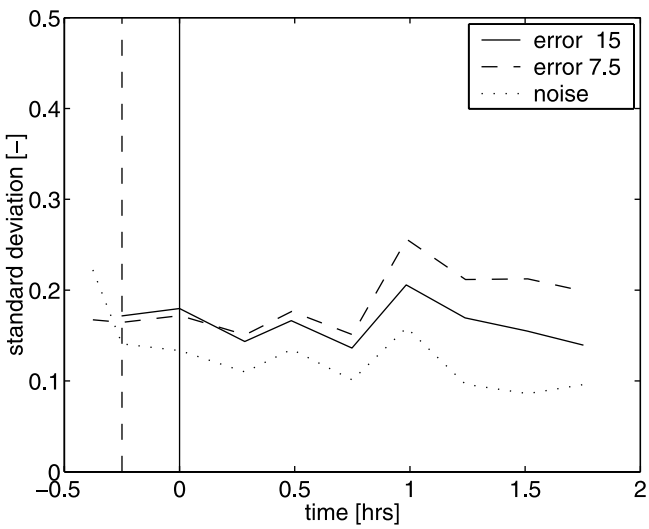

Figure 14. The root mean square error (E_{rms}) for the predictions after 15 min of tuning (solid line) and 7.5 min of tuning (dashed line) compared to an estimate of the standard deviation of the measurement noise (dotted line) for test P0109. Both quantities are scaled by the measured amplitude of the alternate bars. The vertical lines denote the end of the tuning period.

[55] Still, the model can be used to predict the migration of the alternate bars in these experiments. To show this we introduced the data assimilation model, based on a simplified version of the original amplitude evolution model of *Schielen et al.* [1993]. A genetic algorithm can tune this data assimilation model to a number of measured topographies. After tuning, the data assimilation model reproduces the measurements in the Lanzoni experiments very well over a time span significantly larger than the tuning period. Even if only two surveys covering a short time span are used for tuning, the predictions are accurate.

[56] These results do not imply that the theoretical parameters, based on the weakly nonlinear stability analysis, are not useful for predicting alternate bar migration. In the field, with real rivers, the assumption that the width-to-depth ratio is only marginally larger than its critical value may be valid. In that case, the derivation of the amplitude evolution model would be within the validity domain. Consequently, the theoretical estimate of the migration rate may be accurate. In that case, the parameter tuning might be omitted. However, no field information is available so far to test the model against field data.

[57] In the data assimilation model, the amplitude is assumed constant with time, whereas the variations along the channel axis are approximated using an exponentially decaying boundary effect. As this approximation works well in experiment P1801, we conclude that both the length of the flume and the duration of the experiment were too short to allow amplitude modulations to develop. In experiment P0109, there appear to be some changes of the amplitude over time.

[58] The major part of the differences observed between the data assimilation model and the measurements is related to the asymmetry of the alternate bars. The very steep fronts in the flume experiments cannot be reproduced by the second-order approximation used in the model. Higher-order modes are necessary for modeling such steep fronts. This is left for future investigation.

Appendix A: Model of *Schielen et al.* [1993]

$$z_b = \epsilon h_\star A e^{ik_c \frac{x}{h_\star} + \omega_c \frac{t}{T}} \cos\left(\frac{\pi y}{h_\star}\right) + \epsilon^2 A^2 e^{2\left(ik_c \frac{x}{h_\star} + \omega_c t\right)} \left(z_{22s} sin^2\left(\frac{\pi y}{h_\star}\right) + z_{22c} cos^2\left(\frac{\pi y}{h_\star}\right)\right) + \epsilon^2 |A|^2 z_{02} cos(2\pi y) + h.o.t. + c.c. \quad \text{(A1)}$$

$$\frac{\partial A}{\partial \tau} = \alpha_0 A + \alpha_1 \frac{\partial^2 A}{\partial \xi^2} + \alpha_2 |A|^2 A \quad \text{(A2)}$$

$$\tau = \epsilon^2 \frac{t}{T}$$

$$T = \frac{y_\star h_\star}{\sigma\left(\frac{i_b g h_\star}{C_d}\right)^b}$$

$$\xi = \epsilon\left(\frac{x}{h_\star} + \nu_k t\right)$$

$$\alpha_0 = R_c(\tau_r + i\nu_r)$$

$$R_c = \frac{\pi \delta^{\frac{1}{2}}}{C_d}\left(1 + 2\sqrt{\delta} + 4\delta\right)$$

$$\delta = \frac{\gamma C_d}{(b-1)}$$

$$\tau_r = \frac{2\delta(b-1)^2}{\gamma}\left(1 - 4\delta^{\frac{1}{2}} + O(\delta)\right)$$

$$\nu_r = \frac{2\sqrt{2}(b-1)^2 \delta^{\frac{5}{4}}}{\gamma}\left(1 - 3\delta^{\frac{1}{2}} + O(\delta)\right)$$

$$\alpha_1 = -\frac{1}{2}(\tau_{k^2} + i\nu_{k^2})$$

$$\tau_{k^2} = -\frac{8(b-1)\delta^{\frac{1}{2}}}{\pi}\left(1 + 2\delta^{\frac{1}{2}} + O(\delta)\right)$$

$$\nu_{k^2} = -\frac{5\sqrt{2}(b-1)\delta^{\frac{1}{4}}}{\pi}\left(1 - 6\delta^{\frac{1}{2}} + O(\delta)\right)$$

$$\alpha_2 = c_r + ic_i$$

$$c_r = -\frac{2\pi}{3(b-1)} + \frac{(62 - 78b + 19b^2 - 9b^3)\pi}{12(b-1)}\delta^{\frac{1}{2}} + O(\delta)$$

$$c_i = \frac{(20 - 30b + 9b^2)\sqrt{2}\pi}{24(b-1)}\delta^{\frac{1}{4}} + \frac{(-162 + 294b - 133b^2 + 15b^3)\sqrt{2}\pi}{24(b-1)}\delta^{\frac{3}{4}} + O\left(\delta^{\frac{5}{4}}\right)$$

$$\epsilon = \sqrt{\frac{R}{R_c} - 1}$$

$$k_c = \sqrt{2}\pi\delta^{\frac{1}{4}}\left(1 + \frac{19}{4}\delta + O\left(\delta^{\frac{3}{2}}\right)\right)$$

$$\omega_c = -ik_c\left(1 + (b-1)\delta^{\frac{1}{2}} - 5(b-1)\delta + O\left(\delta^{\frac{3}{2}}\right)\right)$$

$$\nu_k = -\left(1 + 7(b-1)\delta^{\frac{1}{2}} - 18(b-1)\delta + O\left(\delta^{\frac{3}{2}}\right)\right)$$

$$z_{02} = -\frac{b}{2(b-1)}\left(1 + (1+b)\delta^{\frac{1}{2}} + O(\delta)\right)$$

$$z_{22s} = \frac{i\sqrt{2}}{3(b-1)}\delta^{-\frac{1}{4}} - \frac{b-2}{3(b-1)} + \frac{i\sqrt{2}(20 - 22b - b^2)\delta^{\frac{1}{4}}}{12(b-1)} + \frac{38 - 59b + b^2}{24(b-1)}\delta^{\frac{1}{2}} + O\left(\delta^{\frac{3}{4}}\right)$$

$$z_{22c} = \frac{-i\sqrt{2}}{3(b-1)}\delta^{-\frac{1}{4}} + \frac{b-2}{3(b-1)} + \frac{i^*\sqrt{2}(20 - 22b - b^2)}{12(b-1)}\delta^{\frac{1}{4}} + \frac{38 - 59b + b^2}{24(b-1)}\delta^{\frac{1}{2}} + O\left(\delta^{\frac{3}{4}}\right)$$

Notation

A	scaled alternate bar amplitude, dimensionless.
b	nonlinearity of sediment transport, dimensionless.
$c.c.$	complex conjugates, dimensionless.
c_b	bed wave celerity, m/s.
c_i	complex part of α_2.
c_r	real part of α_2.
c_1, c_2	boundary layer effect parameters, dimensionless.
C_d	drag coefficient, dimensionless.
C_z	Chézy coefficient, $\sqrt{\mathrm{m}}/s$.
d_{50}	mean grain size, μm.
d_{90}	90% grain size limit, μm.

E_{rms} root-mean-square error of bed level prediction, dimensionless.
g gravity constant, m/s^2.
G nonlinear amplitude correction, dimensionless.
$h_\star$ mean water depth, m.
i_b average longitudinal bed slope, dimensionless.
k the wave number of the alternate bars, dimensionless.
k_c the critical wave number of alternate bars, dimensionless.
k_{nl} the nonlinear part of bed wave number, dimensionless.
K nonlinear wave number correction of bed waves, dimensionless.
NLT nonlinear terms, dimensionless.
Q sediment discharge m^3/s.
R width-to-depth ratio, dimensionless.
R_c critical width-to-depth ratio, dimensionless.
S sediment transport vector, m^2/s.
S_x longitudinal sediment transport, m^2/s.
t time, s.
U flow velocity vector, m/s.
u longitudinal flow velocity, m/s.
$u_\star$ the flow velocity averaged over time and place, m/s.
W nonlinear frequency correction of the bed waves, dimensionless.
x longitudinal coordinate, m.
y transverse coordinate, m.
$y_\star$ channel width, m.
$\tilde{z}_b$ bed level relative to reference point, m.
z_b disturbed bed level relative to mean longitudinal slope, m.
z_{22s} nonlinear bed wave amplitude, dimensionless.
z_{22c} nonlinear bed wave amplitude, dimensionless.
z_{02} nonlinear bed wave amplitude, dimensionless.
α_0 exponential amplitude growth coefficient, dimensionless.
α_1 horizontal amplitude variation coefficient, dimensionless.
α_2 nonlinear amplitude decay coefficient, dimensionless.
Δ relative density of the sediment in water, dimensionless.
δ ratio between frictional and bed slope effects of sediment transport, dimensionless.
ϵ small dimensionless parameter, dimensionless.
η boundary layer effect, dimensionless.
γ downhill preference of sediment transport, dimensionless.
μ bed roughness parameter, dimensionless.
ν_k group speed of the alternate bars, dimensionless.
ν_{k2} real part of α_1.
ν_r real part of α_0.
ϕ_0 phase of the alternate bars, dimensionless.
ρ_s sediment density, g/cm^3.
σ sediment transport proportionality, dimensionless.
τ morphological time, dimensionless.
τ_{k2} complex part of α_1.
τ_r complex part of α_0.
θ shields parameter, dimensionless.
θ_c critical shields parameter, dimensionless.
ξ morphological longitudinal coordinate, dimensionless.
ζ elevation disturbed free surface, m.
ω the frequency of the alternate bars, dimensionless.
ω_c the critical frequency of the alternate bars, dimensionless.
ω_{nl} the nonlinear part of the bed wave frequency, dimensionless.

[59] **Acknowledgments.** The authors thank the Dutch Organisation for Scientific Research (NWO) for funding this work through the "Non Linear Systems" priority program (under project number 620-61-349). It is linked to the EU project HUMOR (number EVK3-CT-2000-00037). Further the authors thank H. J. de Vriend (WL—Delft Hydraulics), A. van Harten (University of Twente) and H. E. de Swart (Utrecht University) for their feedback on this manuscript. We acknowledge K. Sato (Hokaido Research institute) for the alternate bar image.

References

Anderson, R. A., *Optimal Filtering*, Prentice-Hall, Old Tappan, N. J., 1979.
Ashworth, P. J., J. L. Best, J. E. Roden, C. S. Bristow, and G. J. Klaassen, Morphological evolution and dynamics of a large, sand braid-bar, Jamuna River, Bangladesh, *Sedimentology*, *47*, 533–555, 2000.
Canizares, R., A. W. Heemink, and H. J. Vested, Application of advanced data assimilation methods for the initialisation of storm surge models, *J. Hydraul. Res.*, *36*, 655–674, 1998.
Colombini, M., G. Seminara, and M. Tubino, Finite-amplitude alternate bars, *J. Fluid Mech.*, *181*, 213–232, 1987.
Davis, L., *The Handbook of Genetic Algorithms*, Van Nostrand Reinhold, New York, 1991.
De Vriend, H. J., Prediction of aggregated-scale coastal evolution, in *Coastal Dynamics '97*, pp. 644–653, Am. Soc. of Civ. Eng., Reston, Va., 1998.
De Vriend, H. J., Long-term morphological prediction, in *River, Coastal and Estuarine Morphodynamics*, edited by G. Seminara and P. Blondeaux, pp. 163–190, Springer-Verlag, New York, 2001.
Dodd, N., P. Blondeaux, D. Calvete, H. E. De Swart, A. Falques, S. J. M. H. Hulscher, G. Rozynski, and G. Vittori, The use of stability methods for understanding the morphodynamical behaviour of coastal systems, *J. Coastal Res*, in press, 2003.
Feddersen, F., and R. T. Guza, Velocity moments in alongshore bottom stress parametrizations, *J. Geophys. Res.*, *105*, 8673–8686, 2000.
Fletcher, R., *Practical Methods of Optimization*, John Wiley, Hoboken, N. J., 1987.
Furbish, D. J., Irregular bed forms in steep, rough channels: 1. Stability analysis, *Water Resour. Res.*, *34*, 3635–3648, 1998.
Furbish, D. J., S. D. Thorne, T. C. Byrd, J. Warburton, J. J. Cudhey, and R. W. Handel, Irregular bed forms in steep, rough channels: 2. Field observations, *Water Resour. Res.*, *34*, 3649–3659, 1998.
Heemink, A. W., E. E. A. Mouthaan, M. R. T. Roest, E. A. H. Vollebregt, K. B. Robaczewska, and M. Verlaan, Inverse 3D shallow water flow modelling of the continental shelf, *Cont. Shelf Res.*, *22*, 465–484, 2002.
Ikeda, S., G. Parker, and K. Sawai, Bend theory of river meanders. part 1. Linear developement, *J. Fluid Mech.*, *112*, 365–377, 1981.
Johannesson, J., and G. Parker, Linear theory of river meanders, in *River Meandering*, *Water Resour. Monogr. Ser.*, vol. 12, edited by S. Ikeda and G. Parker, pp. 181–214, AGU, Washington, D. C., 1989.
Knaapen, M. A. F., and S. J. M. H. Hulscher, Regeneration of sand waves after dredging, *Coastal Eng.*, *46*, 277–289, 2002.
Knaapen, M. A. F., S. J. M. H. Hulscher, H. J. De Vriend, and A. Van Harten, Height and wave length of alternate bars in rivers: Modelling vs. laboratory experiments, *J. Hydraul. Res.*, *39*, 147–153, 2001.
Lanzoni, S., Experiments on bar formation in a straight flume: 2. Graded sediment, *Water Resour. Res.*, *36*, 3351–3363, 2000a.
Lanzoni, S., Experiments on bar formation in a straight flume: 1. Uniform sediment, *Water Resour. Res.*, *36*, 3337–3349, 2000b.
Leredde, Y., R. I. Dekeyse, and J. L. Devenon, T-s data assimilation to optimise turbulent viscosity: An application to the berre lagoon hydrodynamics, *J. Coastal Res.*, *18*, 555–567, 2002.
Lewis, F. L., *Optimal Estimation*, John Wiley, Hoboken, N. J., 1986.
Meyer-Peter, E., and R. Müller, Formulas for bed-load transport, in *Proceedings of the 2nd Congress IAHR*, vol. 2, pp. 39–64, Int. Assoc. for Hydraul. Res., Delft, Netherlands, 1948.
Moore, A. M., C. L. Perez, and J. Zavala-Garay, A non-normal view of the wind-driven ocean circulation, *J. Phys. Oceanogr.*, *32*, 2681–2705, 2002.

Morelissen, R., S. J. M. H. Hulscher, M. A. F. Knaapen, A. A. N'emeth, and R. Bijker, Mathematical modelling of sand wave migration and the interaction with pipelines, *Coastal Eng.*, *48*(3), 197–209, 2003.

Schielen, R. M. J., A. Doelman, and H. E. De Swart, On the nonlinear dynamics of free bars in straight channels, *J. Fluid Mech.*, *252*, 325–356, 1993.

Sekine, M., and G. Parker, Bed-load transport on transverse slope, *J. Hydraulic Eng.*, *118*, 513–535, 1992.

Seminara, G., G. Zolezzi, M. Tubino, and D. Zardi, Downstream and upstream influence in river meandering. part 2. Planimetric development, *J. Fluid Mech.*, *438*, 213–230, 2001.

Van Leeuwen, P. J., The time-mean circulation in the Agulhas region determined with the ensemble smoother, *J. Geophys. Res.*, *104*, 1393–1404, 1999.

Voorrips, A. C., A. W. Heemink, and G. J. Komen, Wave data assimilation with the Kalman filter, *J. Mar. Syst.*, *19*, 267–291, 1999.

S. J. M. H. Hulscher and M. A. F. Knaapen, Water Engineering and Management, Department of Engineering Technology, University of Twente, P.O. Box 217, 7500 AE Enschede, Netherlands. (s.j.m.h.hulscher@ctw.utwente.nl; m.a.f.knaapen@ctw.utwente.nl)